A nanotube-based field emission x-ray source for microcomputed tomography

J. Zhang and Y. Cheng
Department of Physics and Astronomy, University of North Carolina, Chapel Hill, North Carolina 27599

Y. Z. Lee
Department of Biomedical Engineering, University of North Carolina, Chapel Hill, North Carolina 27599

B. Gao and Q. Qiu
Xintek, Inc. 7020 Kit Creek Road, Research Triangle Park, North Carolina 27709

W. L. Lin
Department of Radiology, School of Medicine, University of North Carolina, Chapel Hill, North Carolina 27599

D. Lalush
Department of Biomedical Engineering, North Carolina State University, Raleigh North Carolina 27695

J. P. Lu and O. Zhou
Department of Physics and Astronomy and Curriculum in Applied and Materials Sciences, University of North Carolina, Chapel Hill, North Carolina 27599

(Received 21 June 2005; accepted 1 August 2005; published online 7 September 2005)

Microcomputed tomography (micro-CT) is a noninvasive imaging tool commonly used to probe the internal structures of small animals for biomedical research and for the inspection of microelectronics. Here we report the development of a micro-CT scanner with a carbon nanotube- (CNT-) based microfocus x-ray source. The performance of the CNT x-ray source and the imaging capability of the micro-CT scanner were characterized. © *2005 American Institute of Physics.* [DOI: 10.1063/1.2041589]

The development of computed tomography (CT) technologies is one of the most important breakthroughs in the field of radiology.[1,2] CT scanners are now widely used for diagnostic medical imaging and security screening. Microcomputed tomography (micro-CT), which is similar to CT but provides a better spatial resolution, has recently emerged as a powerful noninvasive imaging tool for biomedical research[3,4] and for industrial inspection. It has been applied to the high-resolution imaging of bony structures and soft tissues of small animals, materials analysis, and inspection of microelectronics. A typical micro-CT scanner consists of a *microfocus* x-ray source, a sample stage, and an area x-ray detector. A three-dimensional (3D) image of the entire object is reconstructed using the cone-beam reconstruction algorithm[5] from a set of two-dimensional (2D) images recorded over a wide range of viewing angles by either rotating the object or the x-ray source and the detector simultaneously. One of the most critical components of a micro-CT scanner is the microfocus x-ray source. The *spatial* resolution of the micro-CT scanner is largely determined by the focal spot size of the x-ray source. The *temporal* resolution depends on the switching time of the x-ray source, and is important for minimizing motion-induced blurring of moving objects and for gated imaging.

Current commercial microfocus x-ray sources use hot cathodes to generate electrons for x-ray production. The thermionic technology has several inherent limitations. The slow response time limits the *temporal* resolution of the x-ray source. The high operating temperature results in a short lifetime and a large device size. It also requires complex electromagnetic optics to focus the spatially random thermal electrons to provide the small focal spot size required for high spatial resolution. The thermionic microfocus x-ray sources used in the commercial micro-CT scanners typically have an x-ray switching time of 10 ms, effective focal spot size of $5-100$ μm at the beam current of $40-500$ μA, and anode voltage of 30–160 kV.[6]

Field emission x-ray sources can, in principle, offer significantly improved temporal resolution because of the intrinsic instantaneous response time of the field emission process.[7] The design of the microfocus x-ray source can potentially be simplified because of the small divergence of the field-emitted electrons. Field emission x-ray sources based on metal tips have been investigated and tested for clinical uses in the past, but have suffered from a high extraction field and a short lifetime.[8,9] Carbon nanotubes (CNTs)[10] have improved emission characteristics compared to the conventional field emitters.[11–14] It has been shown that they can generate diagnostic quality x-ray radiation[15–17] with temporal resolution up to nanoseconds,[18] which is significantly better than that of the thermionic x-ray tubes.[19] Here we report the development of a micro-CT scanner using a CNT-based microfocus x-ray source and discuss the preliminary results on the performances of the x-ray source and the imaging capability of the micro-CT scanner.

The micro-CT scanner is illustrated in Fig. 1. It com-

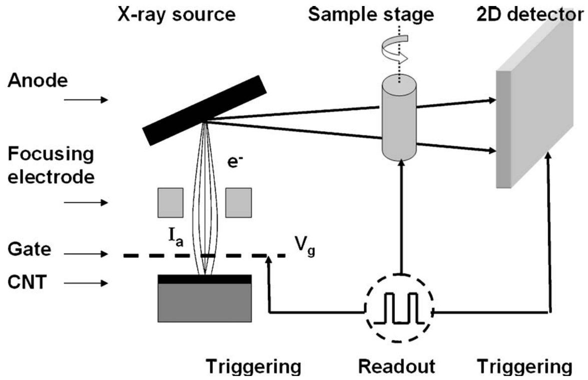

FIG. 1. Schematics of the micro-CT scanner. The source comprises a cathode, a gate and a focusing electrode, and a Mo target at 10^{-7} Torr pressure. The field emission cathode is a 1 mm diam CNT film coated on a metal disk. The digital 2D x-ray image sensor (Hamamatsu C7921) has a 1056×1056 photodiode array with 50×50 μm pixel size and is externally triggered. It can operate at 16 frames per second (fps) when running under a 4×4 binning mode. The source to object distance is 23 cm and the object to detector distance is 3 cm.

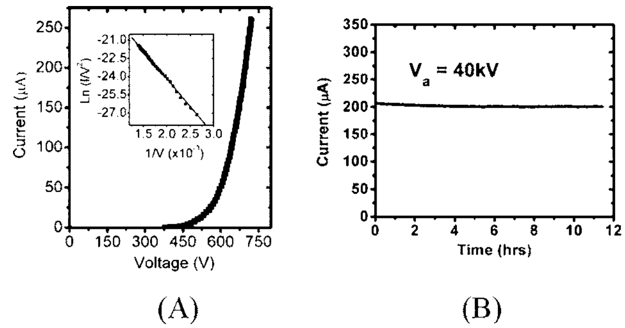

FIG. 2. (A) The x-ray tube current versus the gate voltage measured with the anode voltage fixed at 40 kV. It follows the classic Fowler–Nordheim relation. The distance between the cathode and the gate is 150 μm. (B) The tube current as a function of time at 100% duty cycle and 40 kV anode voltage. The local fluctuation was less than 1% without electronic feedback.

prises a stationary CNT microfocus x-ray source, a motorized high precision sample rotation stage, an optical sensor for the detection of the object position, and a 2D digital x-ray detector. The detector was externally triggered by a transistor–transistor logic (TTL) signal such that the frame speed was the same as the triggering signal. The entire operation of the micro-CT scanner, including x-ray exposure, rotation angle, and data collection, was controlled by a PC using a LabView-based program. A modified Feldkamp cone beam back-projection method[5] written in-house was used for reconstructing the tomographic images from the acquired projection images. The microfocus field emission x-ray source has a triode structure where the x-ray tube current (I_a), which determines the x-ray flux, was controlled by the voltage applied on the gate electrode (V_g), and the energy of the x-ray photon was set by the voltage applied on the anode (V_a). The anode voltage ranges from 0 to 60 kV, which is only limited by the high-voltage power supply (Glassman EW series) used in this experiment. An active focusing electrode, made of a metal cylinder, was placed above the gate electrode to focus the field-emitted electrons. The device operating in the reflection mode was housed in a vacuum chamber with a Be window under a 10^{-7} Torr dynamic vacuum. The emission material used in this study was purified single-wall carbon nanotubes (SWNTs) produced by the laser ablation method at UNC. The cathode was a 1 mm diam uniform layer of randomly oriented SWNTs coated on a metal substrate by electrophoretic deposition with fine control of the film thickness and morphology.[20] A metal grid was used as the extraction electrode.

The emission properties of the gated CNT cathode were characterized at a 10^{-7} Torr vacuum. As shown in Fig. 2(a), field-emitted electrons were extracted when $V_g > 350$ V. The current–voltage relation follows the classic Fowler–Nordheim behavior. An emission current up to 10 mA (~ 1 A/cm^2 density) was obtained at a gate electrical field of ~ 15 V/μm under the pulsed mode. The emission stability and lifetime were tested. After the initial aging process where arcing frequently occurred, the emission current was stable without electronic compensation at current levels required for small animal imaging and V_a up to 60 kV (the highest value tested). Figure 2(b) shows the variation of the emission current versus time measured under the dc mode (100% duty cycle) with fixed V_a (40 kV) and V_g. With a ballast resistor, the emission current decayed from 210 μA to 200 μA over a 12 h period with a local current fluctuation of 0.8%.

Commercial electromagnetic simulation software was used to aid the design of the electron optics. Figure 3(a) shows the simulated electron trajectory using the actual dimension of the experimental system: a 0.6 cm thick Mo anode; a focusing electrode that was 1.5 cm in height and 1 cm in inner diameter; a tungsten grid gate electrode with 25 μm wire diameter, and 81% optical transparency. For the simulation, electrons were launched from the cathode surface and were accelerated by V_g. The deflected electrons transmitted through the gate were focused by the electrostatic field from the focusing electrode. The results show that the focal spot size depends on parameters including the potential, position, and geometry of the focusing electrode, as well as V_g and V_a used.

The dependence of the focal spot size on the potential of the focusing electrode (V_f) was studied by measuring the change in the imaging resolution of a phantom as a function of V_f under fixed V_g using the setup described in Fig. 1. Figures 3(b)–3(d) show the projection images of a computer chip taken at V_f=0, 500, and 700 V, respectively, under otherwise identical conditions (V_a=40 kV, V_g=800 V). Metal wires with a linewidth of 30 μm were resolved at V_f =700 V. The simulation showed that a factor of 4 reduction in the diameter of the electron beam, from 1 mm on the cathode to 250 μm on the anode, was achieved at V_a =40 kV, V_g=800 V, and V_f=600 V. The *effective* focal spot size under these operating conditions was determined experimentally following the European Standard EN 12543-5.[21] A 1 mm diam tungsten wire was placed between the x-ray source and the detector. The profiles of the x-ray beam after passing the W wire were collected with the wire in two orthogonal directions and were analyzed to obtain the effective focal spot size of the source. The measured *effective* focal spot size is 150 μm (horizontal) $\times$ 50 μm (vertical), respectively, consistent with the simulation result.

For tomographic imaging, the exact location of the x-ray

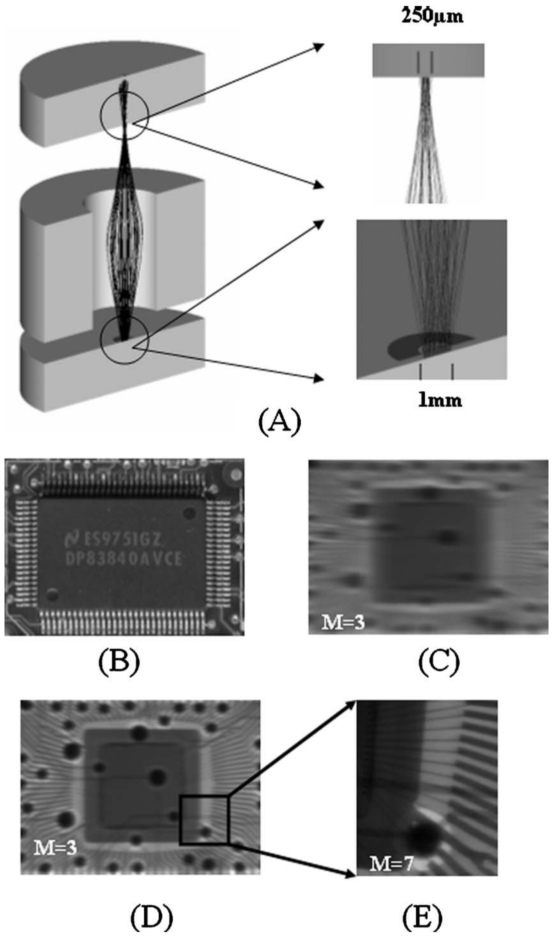

FIG. 3. (a) Computer-simulated electron trajectory using the actual dimension and operating parameters of the x-ray source. The emitting cathode (bottom part) diameter is 1 mm. With a gate at 800 V and a focusing electrode (middle section) at 600 V, the electron beam profile at the anode is 250 μm in size. An *actual* focal spot size of <150 μm was obtained at $V_a=40$ kV, $V_g=800$ V, and $V_f=700$ V. (b) Optical image of a computer chip. (c)–(e) Corresponding x-ray image of the same computer chip under different focusing voltages: $V_f=0$ V, 500 V, and 700 V, respectively. M in the graph represents the magnification factor, defined as the ratio of the image and object dimension, of the x-ray image.

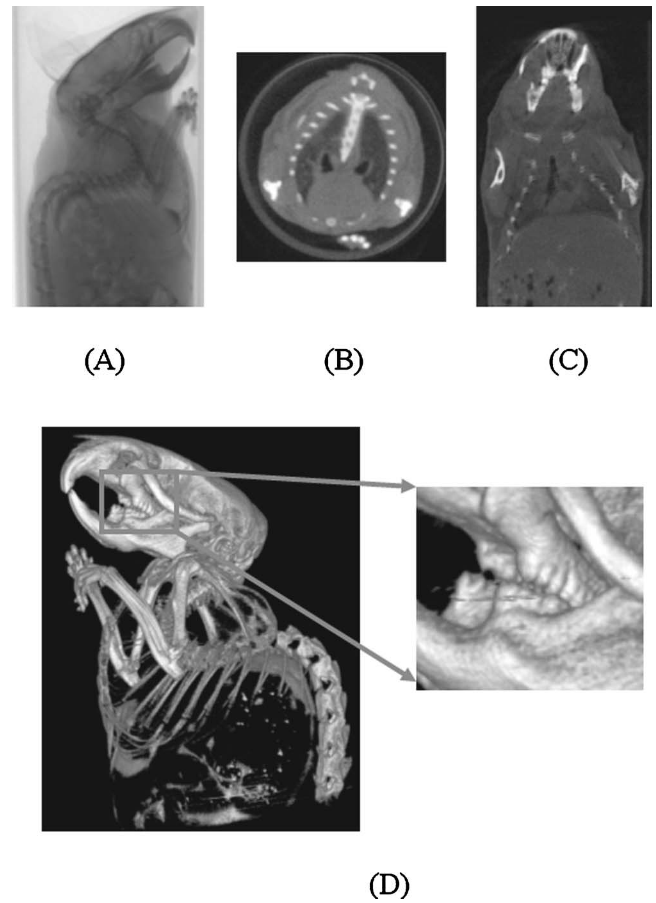

FIG. 4. CT image of a normal mouse carcass (25 g) obtained using the current imaging system. The imaging conditions are 40 kVp, 100 μA tube current, 1 s exposure time, and 150×50 μm effective focal spot size without energy filter. (a) A sample projection image demonstrating good bone delineation and soft tissue contrast. (b), (c) Transverse and coronal micro-CT images of the same mouse clearly show the lungs' location and the separation between low-density fat and surrounding soft tissues. (d) 3D volume rendering of the whole-body skeletal dataset. The bony structures are well visualized, and even small subtle structures, such as the bony sutures in the skull and individual teeth, are readily apparent.

beam center needs to be determined to reduce artifacts in the reconstructed images. This was accomplished by analyzing the distortion of the x-ray projection images of a phantom that contained several equally spaced identical thin metal disks stacked inside a plastic cylinder.[4] Tomographic images of a normal 8-week-old mouse carcass (25 g) were obtained using this micro-CT scanner. To increase the contrast for the soft tissues, an iodinated contrast agent was injected into the abdomen (0.2 ml) of the mouse. A set of 600 projection images was taken over 360° at 1 s exposure per image. The x-ray source was operated at 40 kVp, 100 μA, 150×50 μm effective focal spot size, and cone beam geometry. As shown in Fig. 4(a), the projection images demonstrated good bone delineation and soft tissue contrast. A modified Feldkamp algorithm[5] was used for 3D reconstruction. It took about 3 h to reconstruct a $325\times 325\times 500$ volume at 100 μm pixel size with a single processor on a PC running LINUX. The computing time was subsequently reduced by utilizing multiple processors with a MPI parallelized version of the code. Examples of the tomographic transverse and coronal cuts from the reconstructed volume are shown in Figs. 4(b) and 4(c), respectively. 3D skeletal renderings of the carcass are shown in Fig. 4(d). Due to a much higher x-ray attenuation coefficient in calcified tissue than in soft tissue, the bony structures are well visualized, and even small subtle structures, such as the bony sutures in the skull and individual teeth, are readily apparent. As shown in the figure inset, the image provides sufficient resolution to visualize the individual tooth of the mouse.

In summary, we demonstrate the generation of microfocus x-ray radiation using a CNT-based field emission x-ray source. An effective focal spot size of 50 μm was obtained using one active electrostatic focusing electrode, which can be further reduced with improved design. A micro-CT scanner with the field emission x-ray source was designed and its utility for small animal imaging was demonstrated. The temporal resolution of the system affords potentials for gated and dynamic CT imaging.

ACKNOWLEDGMENTS

This work was partially supported by the NIH (1R21EB004204-01, ONR (MURI), and Xintek, Inc. We acknowledge helpful discussions and assistance from S. J. Oh, S. Dike, S. Chang, and E. A. Hoffman.

[1] G. N. Hounsfield, Br. J. Radiol. **46**, 1016 (1973).
[2] A. M. Cormack, Phys. Med. Biol. **18**, 195 (1973).
[3] M. J. Paulus, S. S. Gleason, S. J. Kennel *et al.*, Neoplasia **2**, 62 (2000).
[4] K. Machin and S. Webb, Phys. Med. Biol. **39**, 1639 (1994).
[5] L. A. Feldkamp, L. C. Davis, and J. W. Kress, J. Opt. Soc. Am. A **1**, 612 (1984).
[6] W. Recheis, preprint.
[7] R. Gomer, *Field Emission and Field Ionization* (Harvard University Press, Cambridge, MA, 1961).
[8] F. M. Charbonnier, J. P. Barbour, and W. P. Dyke, Radiology **117**, 165 (1974).
[9] G. S. Hallenbeck, Radiology **117**, 1 (1974).
[10] M. S. Dresselhaus, G. Dresselhaus, and P. Avouris, in *Topics in Applied Physics* (Springer, Heidelberg, 2000), Vol. 80.
[11] W. A. de Heer, A. Chatelain, and D. Ugarte, Science **270**, 1179 (1995).
[12] A. G. Rinzler, J. H. Hafner, P. Nikolaev *et al.*, Science **269**, 1550 (1995).
[13] P. G. Collins and A. Zettl, Appl. Phys. Lett. **69**, 1969 (1996).
[14] W. Zhu, C. Bower, O. Zhou *et al.*, Appl. Phys. Lett. **75**, 873 (1999).
[15] O. Zhou and J. P. Lu, U.S. Patent 6,553,096, 2003.
[16] H. Sugie, M. Tanemura, V. Filip *et al.*, Appl. Phys. Lett. **78**, 2578 (2001).
[17] G. Z. Yue, Q. Qiu, B. Gao *et al.*, Appl. Phys. Lett. **81**, 355 (2002).
[18] Y. Cheng, J. Zhang, Y. Z. Lee *et al.*, Rev. Sci. Instrum. **75**, 3264 (2004).
[19] E. Sato, M. Sagae, K. Takahashi *et al.*, Med. Biol. Eng. Comput. **32**, 295 (1994).
[20] B. Gao, G. Z. Yue, Q. Qiu *et al.*, Adv. Mater. (Weinheim, Ger.) **13**, 1770 (2001).
[21] CEN/TC, European Standard DIN EN 12543-5, 1999.